GCAGS JOURNAL
A Publication of the Gulf Coast Association of Geological Societies
www.gcags.org

Influence of Stratigraphic Modeling Scales on Shale Oil Resources Assessment of the Midland Basin

Robin Dommisse

Bureau of Economic Geology, Jackson School of Geosciences, University of Texas at Austin, Box X, University Station, Austin, Texas 78713–8924, U.S.A.

ABSTRACT

Modern resource assessment approaches can be greatly aided by integrating all available data and interpretations in a 3D geological model. The model includes stratigraphic, petrophysical, core description, and production data for the Spraberry and Wolfcamp intervals. In this work we highlight the benefits of the development of a high-resolution geomodel for reserves assessment in an unconventional play when compared to more common 2D mapping-based resource play oil-in-place estimation studies. We generated a 3D, faulted Midland Basin geomodel, containing nearly 1.5 billion cells. The model is based on over 2000 correlated wells, 700 wells with petrophysical and facies interpretations, and approximately 10,000 horizontal production wells with decline curve and completion data analyses. This work demonstrates the influence of various vertical stratigraphic resolution scales to the practice of 3D reserves assessment in the Midland Basin.

INTRODUCTION

Two-dimensional mapping-based regional studies can identify general trends related to the distribution of the high total organic carbon (TOC) zones in the Spraberry and Wolfcamp formations but are unable to accurately describe the high degree of heterogeneity of the interbedded carbonate debris flows and the reservoir mudrocks in the Midland Basin. In addition, 2D mapping studies often struggle with capturing the vertical resolution required to characterize the complexity of shelf to basin stratigraphy of the Midland Basin. This study shows how using a high-resolution, integrated 3D geological model can provide a better insight into the relationship between geological and engineering parameters needed to evaluate prospective exploration and development opportunities.

Ten stratigraphic zones, comprised of the Spraberry and Wolfcamp formations, were subdivided into layers with an average cell-thickness of 3 ft and an average lateral cell size of 750 ft by 750 ft, resulting in the creation of a nearly 1.5 billion cell 3D model for the Midland Basin, encompassing an approximately 100 mi by 230 mi area covering 23,000 mi^2. Wolfcampian and Leonardian basinal stratigraphy comprises cyclic successions of siliciclastic and calcareous rocks, which can be distinguished and mapped using wireline logs calibrated against cores.

Manuscript received May 16, 2022; revised manuscript received June 15, 2022; manuscript accepted June 21, 2022.

GCAGS Journal, v. 11 (2022), p. 104–114.

A detailed petrophysical evaluation of wireline logs from 700 wells in the Midland Basin were analyzed (L. Sivila, 2018, unpublished study) to achieve a step-wise solution (RHOMAA [apparent matrix density]—UMAA [apparent matrix photoelectric effect]) using triple combination well logs, including the photoelectric factor. Petrophysical log properties calculated in this study include TOC, kerogen density, clay volume, non-clay lithology, total porosity, and total water saturation.

Quantifying the stock tank oil initially in place (STOIIP) is necessary for making an analysis of the resource potential as well as the technically recoverable reserves of the Midland Basin. Seven separate 3D model scenarios of varying vertical stratigraphic layer resolution were constructed to test the influence of well log resampling on reserve-calculations. Total porosity and total water saturation were distributed using facies-conditioned kriging to calculate the reserves-in-place scenarios.

This study describes the construction of a high-resolution regional 3D geocellular model of the Midland Basin to gain a deeper understanding of the reservoir architecture using a combination of well log, core, and production data. We used industry-standard petrophysics and 3D modeling software. The two major objectives aided by this model are: (1) Assessing the hydrocarbon reserves-in-place using detailed geological, fluid, and rock properties; and (2) Utilizing the model to investigate how different scales of stratigraphic zonation affect the calculation of original oil in place values.

GEOLOGICAL SETTING

The Midland Basin forms the eastern sub-basin of the Permian Basin in West Texas and southeastern New Mexico. The

deep-water basin is bounded by carbonate platforms, which originated from pre-Permian structural uplifts—the Central Basin Platform, the Northern Shelf, and the Eastern Shelf. The Permian Basin extends over an area of more than 100,000 mi^2. The Midland Basin's stratigraphic framework is increasingly well understood as a result of geological investigations associated with a century-long history of petroleum exploration (Ruppel, 2019, 2020).

The lower Permian Spraberry-Wolfcamp interval is more than 2000 ft thick, (Hamlin and Baumgardner, 2012), and has been developed using multistage, hydraulic-fracture stimulation treatments, through which large volumes of reservoirs are accessed and produced. The Wolfcamp is a complex formation, comprised largely of organic-matter-rich hemipelagic mudrocks and argillaceous carbonates, alternating with subaqueous gravity-flow deposits sourced from the platforms surrounding the basin (Ruppel, 2019, 2020). Basinal sedimentation was controlled by sea-level changes. During periods of high relative sea-level, carbonate debris flows and turbidites were the main external sediment input, whereas during periods of low relative sea-level the sediment was largely siliciclastic in character. Currently the Wolfcamp is being developed as a stacked pay with multiple landing zones for horizontal wells being drilled from the same well pad. These zones are typically designated by operators (from uppermost to lowest) as the Wolfcamp A, B, C, and D (Sinclair, 2017).

METHODOLOGY

Stratigraphic Framework

The Midland Basin is one of the most densely drilled basins in the world, and consequently a rich geological and petrophysical database is potentially available for the construction of a 3D geomodel. Unfortunately, much of the data is proprietary. The dataset includes access to the IHS Permian Basin well and log curve database via a subscription, IHS completions and production data, and Texas Railroad Commission (RRC) well data. The IHS database for the basin contains over 122,000 wells. A multidisciplinary team of geoscientists and engineers contributed and interpreted additional data for the 3D Midland Basin model.

Stratigraphic interpretations, from the Upper Spraberry through the Wolfcamp down to the Strawn, formed the geological framework of the Midland Basin 3D model. This model was based on correlation of wireline logs carried out for over 2000 wells (Hamlin and Baumgardner, 2012; and additional unpublished data from H. S. Hamlin). Trends from horizontal well landing zones were used in this model to constrain the interwell stratigraphic and structural horizon interpretations, based on the methodologies described in Dommisse (2021).

Building the 3D Models

An initial, base case 3D model was built to cover the Midland Basin area. Ten stratigraphic zones, including the Spraberry and Wolfcamp subunits, were subdivided into layers with an average vertical cell thickness of 3 ft. Approximately 9700 horizontal wells were imported into the model. These wells were drilled by operators to develop the producing formations using hydraulic fracture completion techniques. Regional faults for the Midland Basin (Ruppel, 2019, 2020) were converted to 3D vertical fault planes containing vertical fault separation interpretations. Combining these faults with the stratigraphic horizons resulted in the creation of a sealed faulted framework for the 3D geocellular model. This base case 3D geocellular model contains nearly 1.5 billion cells. Figure 1 displays a 3D view from the south of a fence diagram consisting of north-south and west-east cross-sections from the average 3 ft thick layer 3D model, showing calculated bulk volume hydrocarbon volume (BVH) based on distributions of facies-conditioned porosity and water saturations

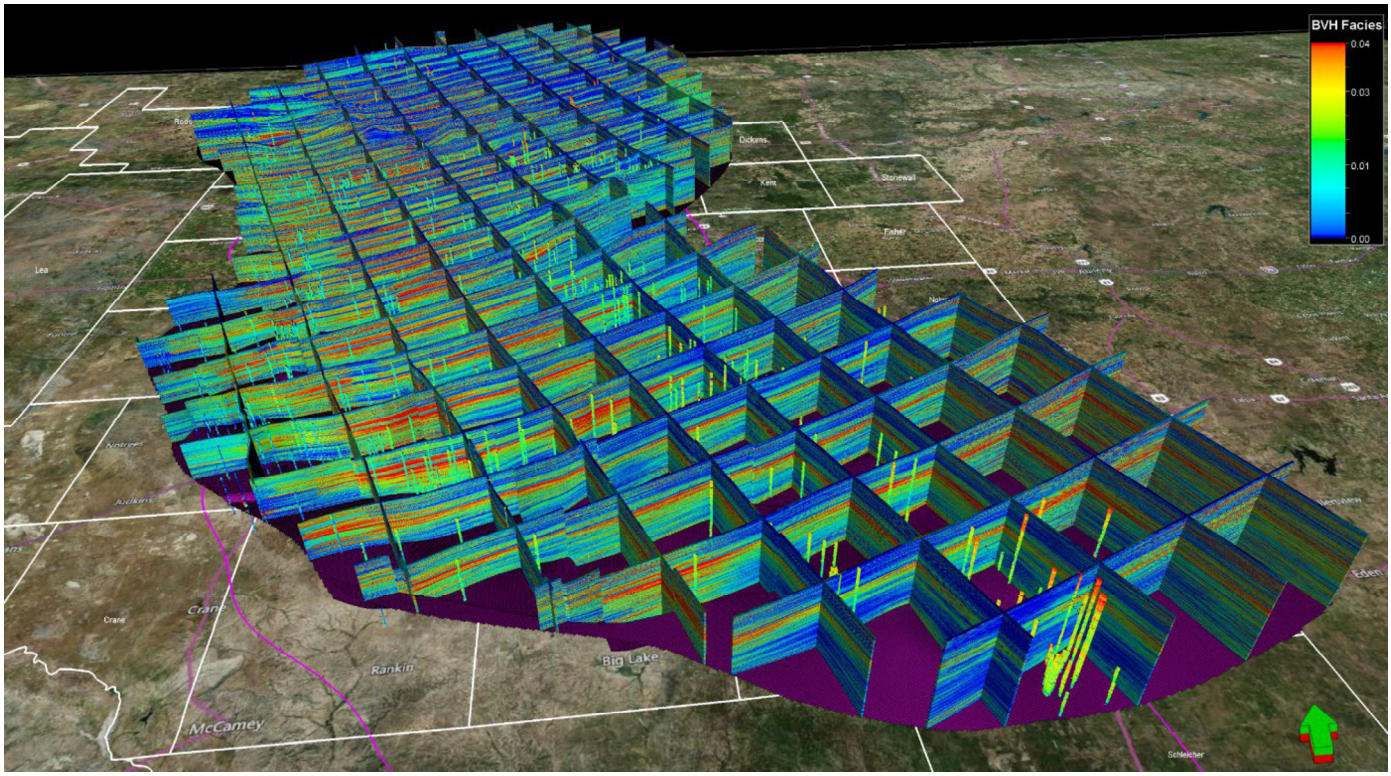

Figure 1 displays a 3D view from the south of a fence diagram consisting of north-south and west-east cross-sections from the 3D model, which contains 1020 layers with an average thickness of 3 ft.

for the Spraberry and Wolfcamp intervals. The red- and yellow-colored cells represent high values of BVH and the green and blue colors show low values of BVH. The fence diagram is bounded by the base of the Wolfcamp D (purple surface).

Multiple 3D Model Scenarios

We created seven different versions of the 3D geological model, by copying the base case 3D model, keeping all input and control parameters fixed and only varying the average vertical cell thickness (Table 1). All workflow steps described in this section, from stratigraphic framework generation to STOIIP calculation, were repeated for each of the models. The purpose of creating the multiple vertical resolution scenarios is to test the influence of well log averaging and stratigraphic correlation framework resolution on STOIIP calculations.

Lithofacies Determination and Distribution

Wolfcampian and Leonardian basinal stratigraphy (Hamlin and Baumgardner, 2012) comprises cyclic successions of siliciclastic and calcareous rocks, which can be distinguished and mapped using wireline logs and cores. Specific lithofacies or groups of related lithofacies are identified using a cutoff method on gamma ray and resistivity log curves (Hamlin and Baumgardner, 2012). The gamma ray–resistivity cutoff method provides a "quick look" lithology determination for correlation and was used to identify three main facies classes (H. S. Hamlin, unpublished dataset). Facies 1 (clay-rich mudrock) is composed mainly of clay-rich shale, siltstone, and sandstone (variable gamma ray and low resistivity). Facies 2 (organic-rich mudrock) is composed of siliceous and calcareous mudrocks that are clay-poor and organic-rich (high gamma ray and high resistivity). Facies 3 (carbonate) is composed primarily of detrital limestone (low gamma ray and high resistivity).

The next step involved resampling the discrete facies curve, defined every half foot, at the resolution of each of the 3D models (e.g., average 3 ft vertical layer thickness for the base case model). We calculated experimental variograms for each of the three facies for the stratigraphic zones, resulting in 30 individual facies variograms, providing parameters including sill, nugget, and range for each of the zones. Next, we calculated the vertical proportion curves for the three facies for the stratigraphic zones. Finally, we used the variogram and vertical proportion curve parameters to distribute the facies using an indicator kriging algorithm. In the base case 3D model with average 3 ft thick layers, this resulted in the creation of 1020 facies maps from the top of the Spraberry to the base of the Wolfcamp D.

The west-east equal-distance cross-section in Figure 2 shows the modeled interwell three-facies model distribution along with well log templates containing gamma ray, resistivity, and stratigraphic zone logs. Rapid changes in the vertical facies successions can be observed in the five smaller facies maps at the base of the figure, illustrating the change in vertical and lateral facies distributions when stepping down through the Middle Leonard Formation, showing a selection of 3 ft thick layers.

Petrophysical Analysis

Petrophysical well logs for 700 wells were calculated using the RHOMAA–UMAA method (Doveton, 2014) using triple combination well logs, including the photoelectric factor. The RHOMAA–UMAA method was successfully compared to multimineral solutions and determined to be a robust solution for wells with basic log data. The raw petrophysical well log curves include gamma ray, resistivity, density, neutron-porosity, and photoelectric constant (PE) curves. The calculated petrophysical log properties derived from the RHOMAA–UMAA method include TOC, kerogen density, clay volume, sand/silt volume, carbonate volume, total porosity, and total water saturation.

The petrophysical source and calculated curves were integrated into the 3D model through vertical resampling at the resolution of each of the 3D models (e.g. average 3 ft vertical layer thickness for the base case model). Figure 3 shows five different fence diagrams, viewed from the southwest, displaying different distributions of these petrophysical and facies attributes, including TOC, volume of clay, volume of kerogen, and volume of sand. The horizontal producer wells are shown in the areas between the cross-sections, colored by landing zone.

Variograms and vertical proportion curves of the petrophysical well logs were computed to quantify the vertical and horizontal spatial variability for each of the facies in the stratigraphic zones. The petrophysical values were then distributed laterally using different algorithms, including facies-conditioned kriging, moving average, and sequential Gaussian simulation. The facies-conditioned kriging distributions for total porosity and total water saturation were selected to calculate the reserves-in-place scenarios.

Calculating and Distributing Pressure and PVT Data

Initial pore pressure was estimated based on instantaneous shut-in pressure (ISIP) and Poisson's ratio logs using a method utilized by Pioneer Natural Resources in the Midland Basin (Friedrich and Monson, 2013). Pore pressures for the available ISIP wells were converted to a gradient of psi/ft, assigned to lo-

Table 1. 3D model scenarios.

Average Layer Thickness (ft)	Number of Model Cells (millions)	Number of vertical layers	Comments
370	14.4	10	Single layer per zone
180	26.0	18	
120	49.2	33	
60	85.2	59	
30	161.7	112	
10	491.0	340	
3	1473.0	1020	Base case model

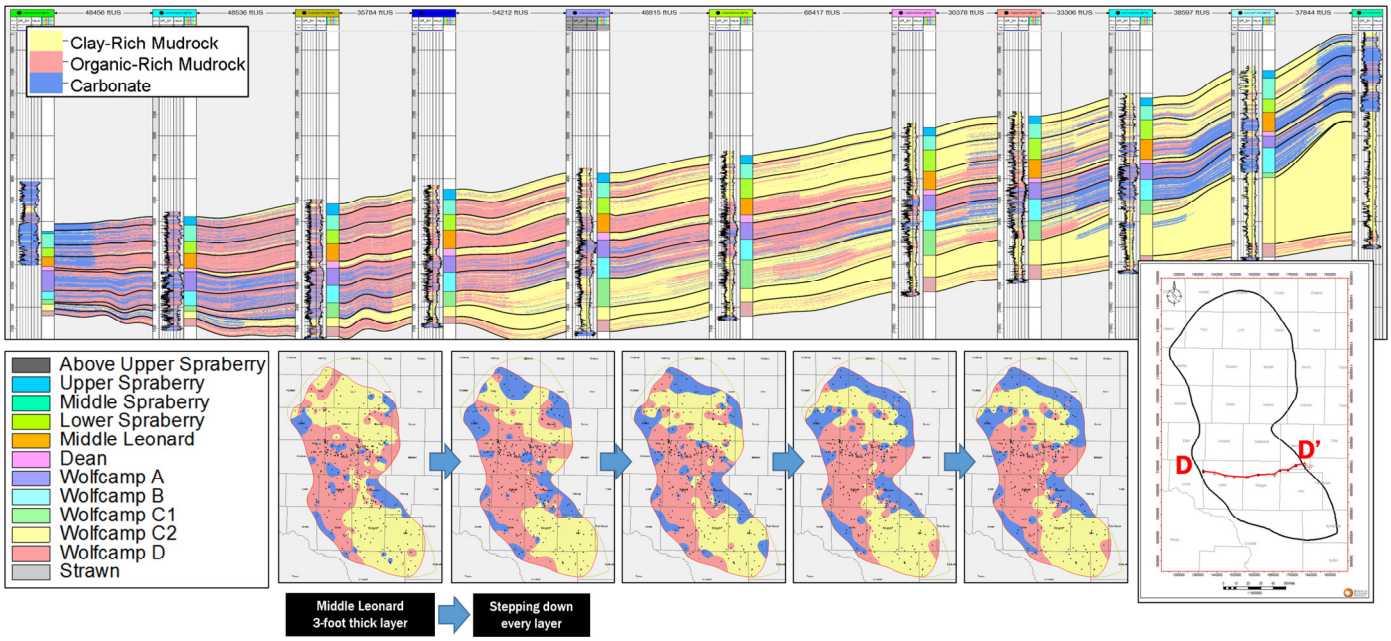

Figure 2. Midland Basin facies distribution. The west-east cross-section shows the interwell facies distribution along with well log templates containing gamma ray, resistivity, and stratigraphic zone logs. The five smaller facies maps illustrate the change in vertical and lateral facies distributions when stepping down through the Middle Leonard Formation, showing a 3 ft thick layer at a step-interval of 3 ft .

cations at the midpoints of the horizontal producer legs, and subsequently distributed using a kriging algorithm along the stratigraphic zones of the 3D model. Reservoir pressure for each 3D model cells was calculated from the distributed pore pressure gradients by multiplying the vertical depth-to-surface distance with the pressure gradient and adding the standard surface pressure.

Analysis of pressure, volume, and temperature fluid properties (PVT) for Wolfcamp oil samples identified the need to develop two fluid models to characterize the oils in the Midland Basin (Gherabati, 2018). These models were based on the range of API gravity, solution gas-oil-ratio, and pressure cutoffs for these oils. API gravity values were assigned to locations at the midpoints of the horizontal producer legs and were then distributed along the stratigraphic zones of the 3D model using a kriging algorithm. Formation volume factors and pressure curves were generated for both fluid models using the 3D model equation-based calculator (Fig. 4).

Oil-in-Place Volume Calculations

We calculated BVH based on distributions of facies-conditioned, kriged total porosity and total water saturations. BVH (fraction) is calculated using total porosity (ϕ, fraction) and total water saturation (S_w, fraction):

$$BVH = \phi(1 - S_w) \quad (1)$$

Stock tank oil initially in place (STOIIP, stock tank barrels) is calculated using total porosity (ϕ, fraction), cell volume (V, cubic feet), total water saturation (S_w, fraction), and oil formation volume factor oil (B_o, reservoir barrel/stock tank barrel). 5.615 is the conversion factor from cubic feet to barrels (bbls):

$$STOIIP = \frac{\phi\, V\, (1-S_w)}{5.615\, B_o} \quad (2)$$

Porosity and water saturation for both calculations were obtained from the facies-conditioned, kriged total porosity and total water saturation distributions. We converted the oil formation factor (B_o) versus pressure curves from the crossplot in Figure 4 to Petrel equations to calculate oil formation volume factor in every cell. We used these formation volume factor distributions and a conversion factor from cubic feet to barrels (5.615) to obtain STOIIP values (Eq. 2). We used cutoffs consisting of volume of clay < 30%, volume of kerogen > 2%, and BVH > 2%. The BVH cutoff corresponds to a porosity cutoff of 5% and an oil saturation cutoff of 40%. Identification of potential pay intervals was based on the intervals with highest BVH, highest kerogen volume, and the lowest clay volume (Heape, 2017). We applied the cutoffs and summed the net reservoir STOIIP as well as the gross volume STOOIP for a single-county subset of the various models. Next, we cross-plotted these results versus the average layer thickness used for the model scenarios. Finally, the STOIIP values were summed by zone and model scenario and summarized for each stratigraphic interval using the three separate facies distributions (Fig. 5).

We quantified the sensitivity of the calculated STOIIP values to a range of combined input data cutoffs, including volume of clay, volume of kerogen, and BVH, using multiple scenarios (Fig. 6). The upper left image shows a fence diagram with the data cutoffs applied. The horizontal producing well trajectories are colored by landing zone in this image. The cross-section image in the upper-right part of the figure shows the gross BVH without any applied cutoffs, and the bottom-right image shows the cells corresponding to the combination of cutoff values. Both cross-sections show overlays of well log curves, with gamma ray shown on the left, increasing to the left, and resistivity shown on the right, increasing to the right. Red colors represent higher values for both gamma ray and resistivity, and blue colors represent lower values for the log curves.

An additional STOIIP sensitivity study to petrophysical parameters was undertaken with the help of cumulative STOIIP distribution functions, cross-plotting STOIIP, porosity and water saturation for each of the three facies distributions in the ten 3D model stratigraphic zones. 3D attribute distributions were ex-

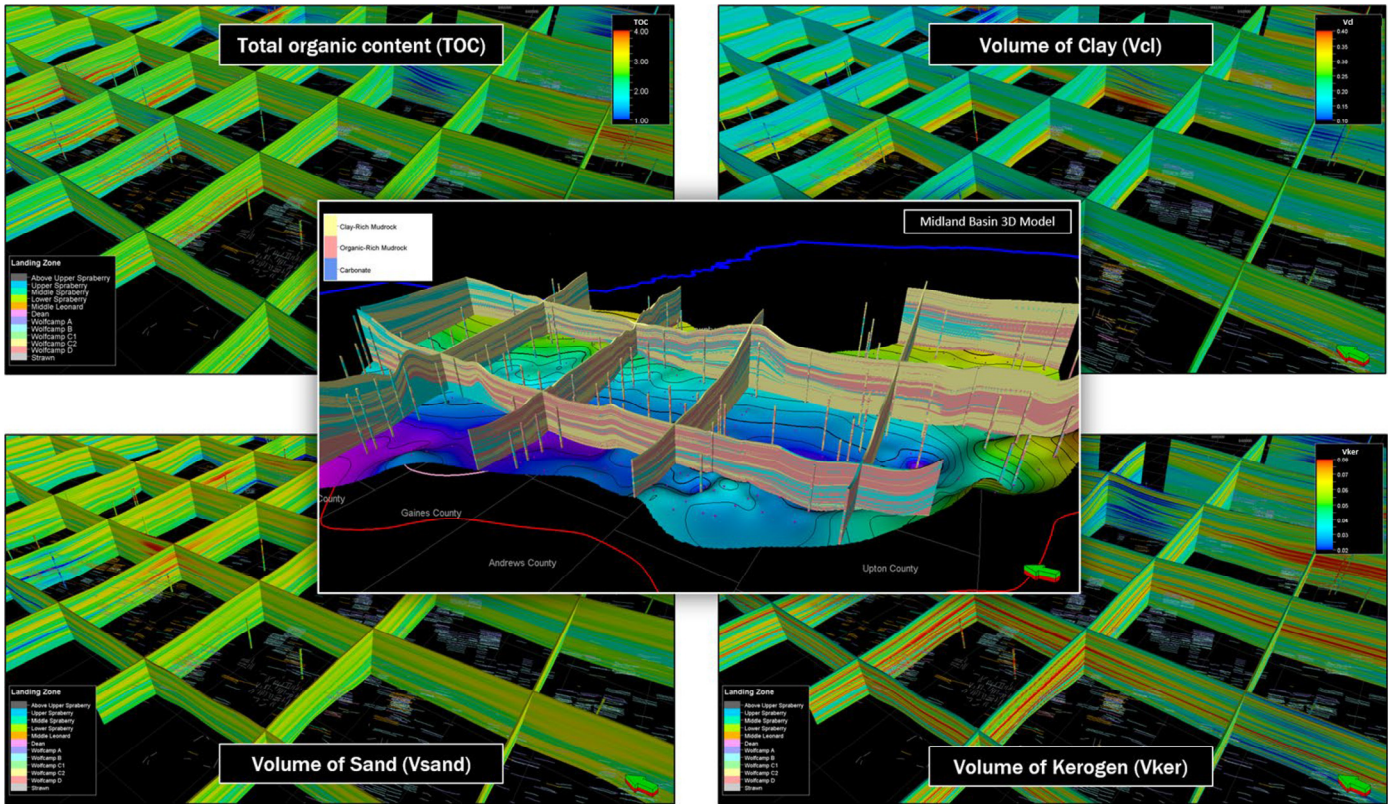

Figure 3. Midland Basin 3D model containing nearly 1.5 billion cells, each with an X and Y increment of 750 ft and an average cell thickness of 3 ft. The fence diagram in the center image shows facies distribution. The four background images illustrate different petrophysical distributions obtained from the petrophysical analysis.

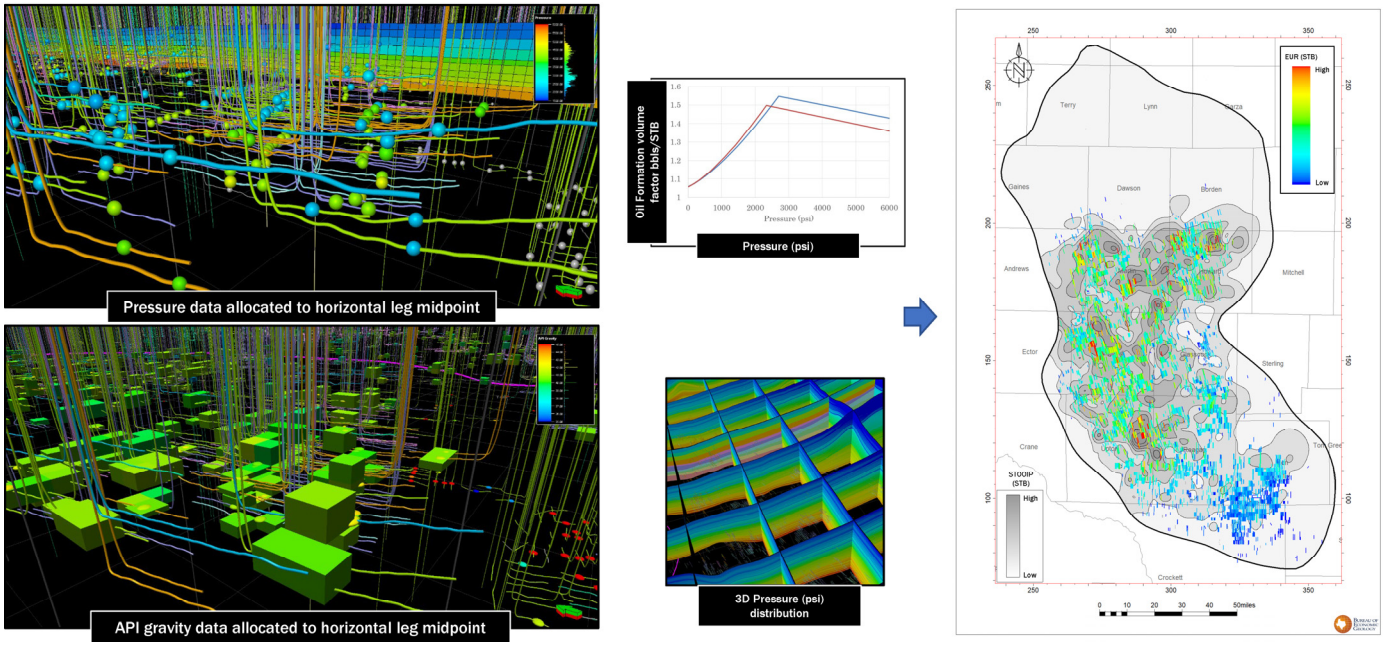

Figure 4. Midland Basin pressure and API gravity distribution. The upper-left image shows the location of the pressure-gradient data obtained from the ISIP calculation. The API gravity values were also assigned to midpoints in the horizontal producer wells. The formation volume factor versus pressure chart shows the two fluid models used in the 3D model. The map on the right shows a resulting STOOIP example from the 3D model with an overlay of the estimated ultimate recovery (EUR) values for all of the horizontal wells used in this study.

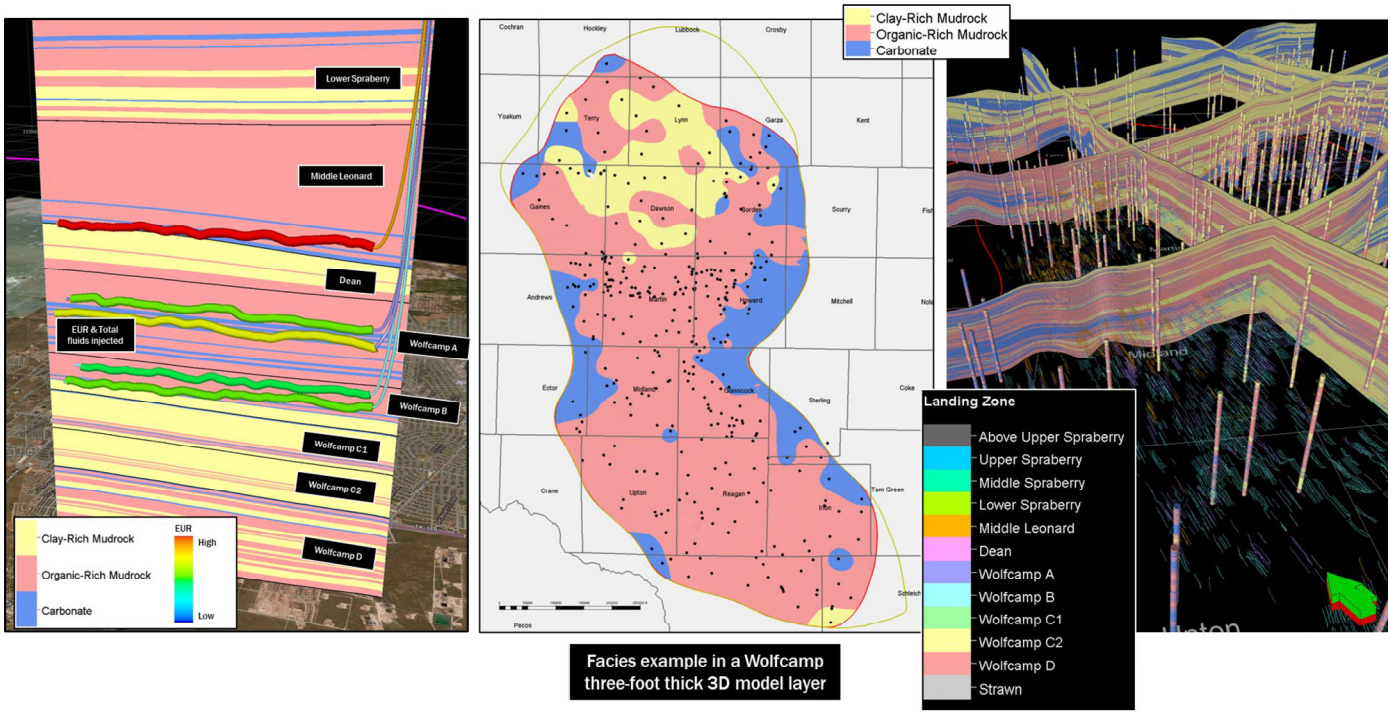

Figure 5. Midland Basin facies distribution. The image on the left shows a cross-section following the lateral trajectory of several vertically stacked horizontal wells targeting multiple zones. The well trajectories are colored by EUR obtained from decline curve analysis. The middle image shows a 3 ft thick stratigraphic layer from the 3D model, along which the facies values have been distributed using indicator kriging. The symbols represent the wells containing facies interpretations. The right image shows a facies fence diagram with the vertical facies wells together with producing horizontal well trajectories colored by landing zone.

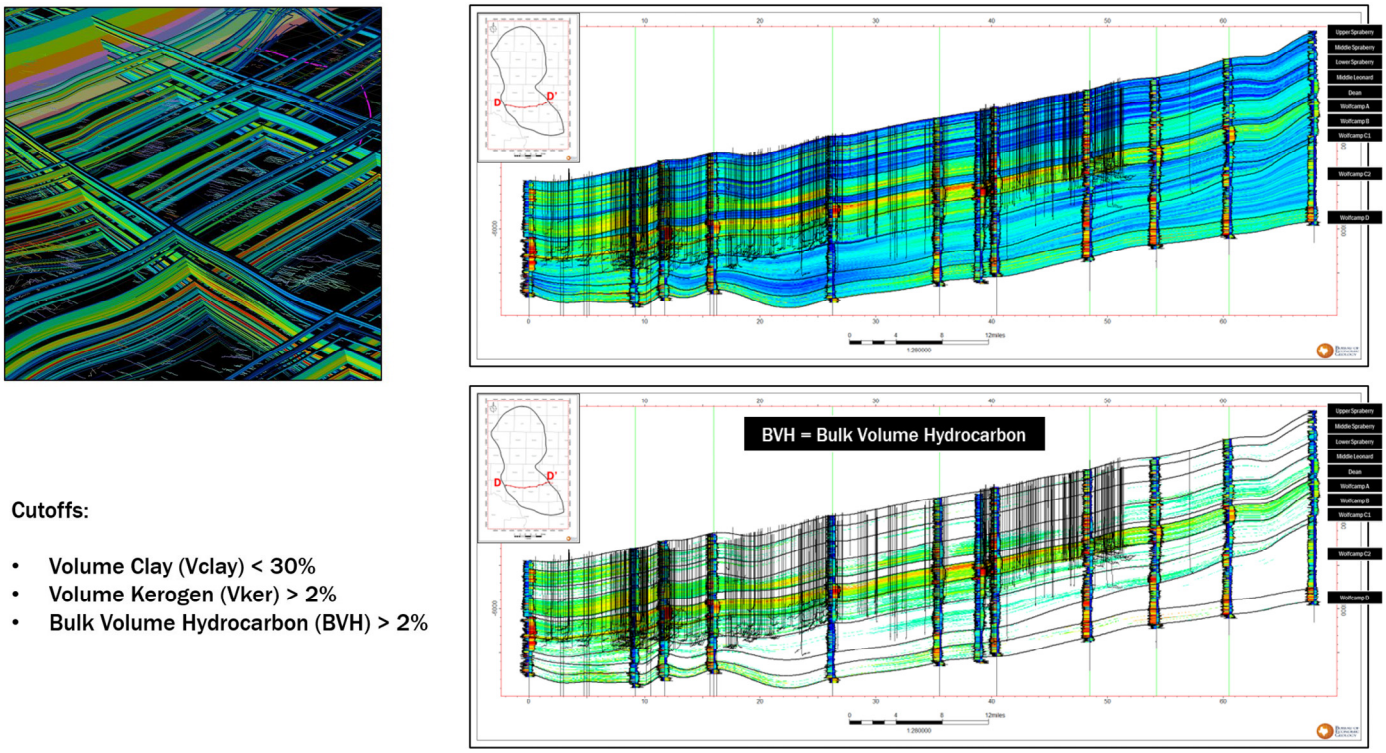

Cutoffs:

- Volume Clay (Vclay) < 30%
- Volume Kerogen (Vker) > 2%
- Bulk Volume Hydrocarbon (BVH) > 2%

Figure 6. Midland Basin reserves assessment—STOIIP with cutoffs. The image in the upper left shows a 3D fence diagram of BVH after applying the cutoffs described above. The horizontal producing well trajectories are colored by landing zone. The two images on the right show a west-east cross-section through the southern part of the Midland Basin displaying BVH calculated for each model cell. The lower image shows the BVH distribution with these cutoffs applied. Left log curve is gamma ray increasing to the left. Right log curve is resistivity, increasing to the right. Horizontal well trajectories are shown as black lines. Vertical exaggeration is 20x.

ported from the 3D model, which were processed using the Python scripting language, and the Dask package (Male, 2018).

The 3D model STOIIP values were summed up for each of the individual facies in each of the zones. Figure 7 shows the STOIIP values in an example layer from the Middle Leonard for each of the three-facies classes, from left to right; organic-rich mudrock, clay-rich mudrock, and carbonates. The horizontal wells are overlaid onto the STOIIP maps and are colored by estimated ultimate recovery (EUR). Monthly oil, water, and gas production and injection data were obtained from a variety of sources, including IHS Enerdeq, the RRC, and DigitalH_2O. These production data were integrated with the 3D model and used to cross-correlate geological parameters with engineering and production data. Ultimate recovery estimates were generated from the production data for each phase, using the physics-based model of Male (2019), modified for Midland fluid properties. We used the 3D model as a tool to quickly compare production data such as total fluids injected, EUR, and watercut with the geological and petrophysical data including zonation, facies, porosity, and water saturation (Male, 2018).

RESULTS

Seven 3D models for the Midland Basin containing distributions of petrophysical well logs, facies, and fluid properties have been built in Petrel. The 3D models' average thickness interval, measured from the top of the Upper Spraberry to the top of the Wolfcamp D is 3000 ft, with a thickness range between 1100 and 5000 ft (true vertical thickness).

Analysis of the 3D model facies distribution shows that clay-rich mudrock (facies 1) occurs primarily in the upper and lower Spraberry, Dean, and Wolfcamp C. Organic-rich mudrock (facies 2) occurs primarily in the middle Spraberry, middle Leonard, and Wolfcamp A and B. Carbonate facies 3 occurs near basin margins in all zones (Hamlin and Baumgardner, 2012). Cross-sections derived from the model describe the facies architecture by showing the overall continuity and connectivity of the three facies distributions (Fig. 2).

The results of the petrophysical interpretations shown in Figure 3 are consistent with the geological framework, core data measurements and other public information. The interpreted rock properties are consistent with those of a tight rock play, with porosity typically less than 15%, clay volume less than 40%, TOC values less than 10%, and high water saturations above 40%.

3D Model and Horizontal Producers

The image on the left of Figure 5 shows a facies cross-section following the trajectories of several vertically stacked horizontal wells, targeting multiple zones in both the Spraberry and Wolfcamp formations. The well trajectories are color coded by EUR obtained from decline curve analysis (Male, 2019). The middle image shows a three-foot thick stratigraphic layer from the 3D model, containing facies values that been distributed using indicator kriging. The symbols represent the wells with facies interpretations. The right image in Figure 5 shows a fence diagram displaying the three-facies distribution along with the trajectories of producing horizontal wells colored by landing zone. Calculation of average facies thickness vertically by zone presents additional data about possible shifts in reservoir continuity vertically through the study area (Price, 2021).

The 3D model stratigraphic framework provides quality control for the reported landing zones for approximately 9,700 producing horizontal wells. Comparisons of the relative position of the landing zones reported by operators to the regulators (Texas Railroad Commission, 2022) with the stratigraphy represented in the geocellular model were made for approximately 9700 producing horizontal wells. Landing zones for the wells targeting the ten stratigraphic zones of the Spraberry-Wolfcamp interval were determined by calculating the intersection between the well trajectories and the 3D model zones on a foot-by-foot basis to yield the most-abundant stratigraphic zone traversed by the horizontal wells. The well trajectories shown in Figure 8 are colored by the stratigraphic zone intersected by the well paths. The distribution of stratigraphic landing zones for the 9700 hori-

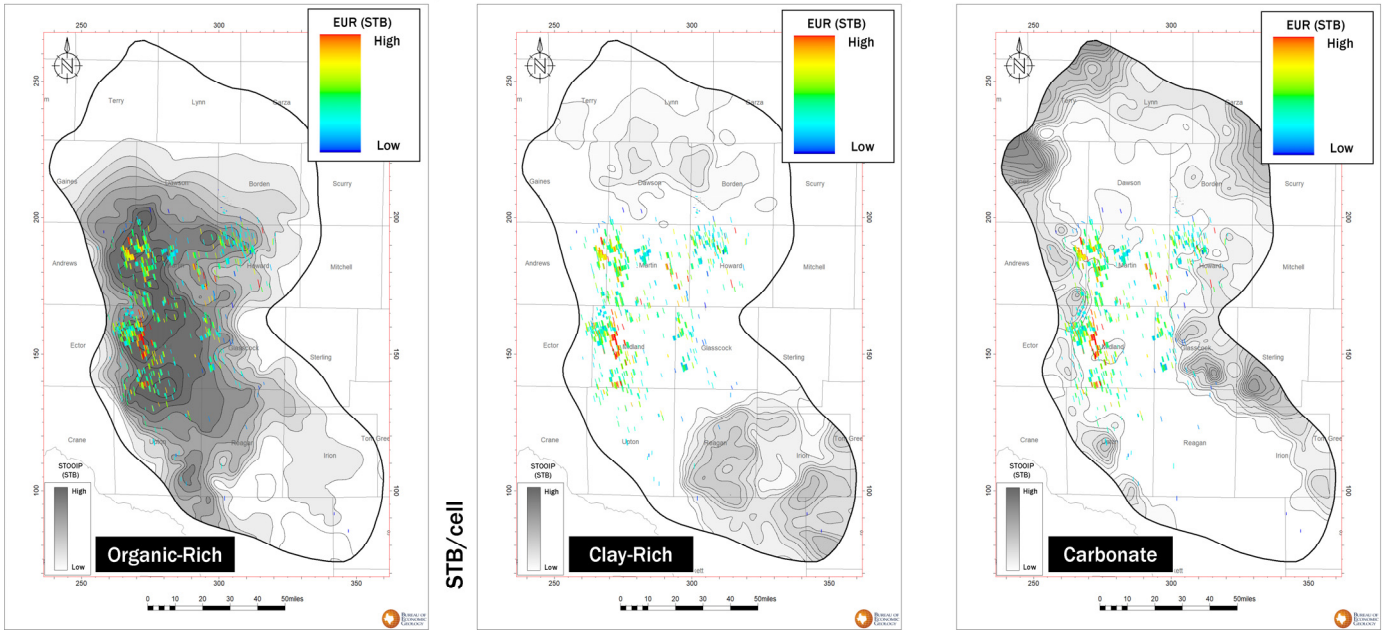

Figure 7. STOIIP by facies per formation. The left image shows the stock tank initially in place values for the organic-rich mudrock facies distribution in an example layer from the Middle Leonard. The trajectories for the producing horizontal wells landed in the Middle Leonard are colored by EUR. The maps are repeated to the right for the clay-rich and carbonate facies distributions in the Middle Leonard example layer.

zontal wells in this study are shown by the histogram in this figure. This process identified the Wolfcamp A and B as the main zones targeted by Midland Basin operators (Fig. 8).

Analysis of the pressure distributions, obtained from the ISIP study, identified the Wolfcamp as an overpressured reservoir since the pressure gradients are greater than the hydrostatic gradient. Historically, the Spraberry Formation has been documented as being underpressured (Friedrich, 2013), a fact which was confirmed by the pore pressure gradient distribution of the 3D model in this study (Fig. 4).

Production and engineering data was integrated with the 3D model, which we used to cross-correlate geological parameters with well performance. Figure 9 shows various production data and completion metrics collected for each of the horizontal wells. The colored surface showing structural contours is the top of the Wolfcamp C1 zone. The well trajectories are colored by different operators. The cube shape at the heel of the well shows colors representing total fluids injected. The 3D ellipsoids at the midpoint of the lateral segment of the well are colored by EUR. The watercut of the well for a particular monthly time-step is shown as a pie diagram at the toe of the wells for which we have production data available. The color of the cylinder along the lateral segment of the well represents the stratigraphic landing zone of the well. In the background we display several cross-sections along several horizontal well trajectories, showing stratigraphic zones and facies. The cross-section shown in the far background shows the distribution of porosity in the zones above the Wolfcamp C1. The vertical grey surface in the middle of the image represents a west-east trending fault expressed in the Wolfcamp C1 horizon. Note the influence of the fault zone on the horizontal well trajectories traversing the fault zone from both the north and the south (Fig. 9).

STOOIP and Stratigraphic Resolution

Modern 3D modeling software has made it easier to create and manage multiple 3D model versions which gave us the ability to compare vertical and lateral variability of BVH calculations based on two vertical stratigraphic resolution scenarios (Fig. 10). The top cross-section was taken from a single-layer per formation 3D geocellular model, comparable to current 2D mapping-based reserves evaluation studies. The bottom cross-section was taken from the high-resolution geocellular model. The two 3D cross-sections on the left show the corresponding vertical resolutions for an area containing multiple stacked horizontal wells. The horizontal sections of the producing wells are colored by EUR. The cross-section colors represent the BVH values. A satellite image is shown at the base of both images (Bing Maps, 2022).

Using the 3D model, the sensitivity of the results to the number and thickness of vertical cells used to resample the petrophysical well log curves was investigated. We applied a set of cutoffs designed to identify the recoverable reserves based on the following criteria: clay volume < 30%, kerogen volume > 2%, and BVH > 2%. We repeated this workflow to produce a series of seven individual 3D models increasing vertical resolutions (i.e., decreasing average layer thicknesses). The average layer thickness scenarios for the top of Spraberry to base of Wolfcamp D interval ranged from 3 ft to 370 ft. The latter number represents the average thickness of the layers for the scenario where we used a single layer for each of the ten formations in the 3D model.

Comparing a variety of 3D model reserve calculations for an area of the model, ranging from a lower-resolution 14 million cell model to the nearly 1.5 billion cell model, showed total gross-pay calculated STOIIP ranges between 179 and 189 billion stock tank barrels (STB). The total net-pay calculated STOIIP ranges between 111 and 127 billion STB (Fig. 11).

Petrophysical properties were extracted from the geomodel in the GSLIB format. A Python script using the Dask package was used to assign average petrophysical properties from a 20 ft radius about the midpoint of each producing horizontal well. These extracts can be combined with completion and drilling

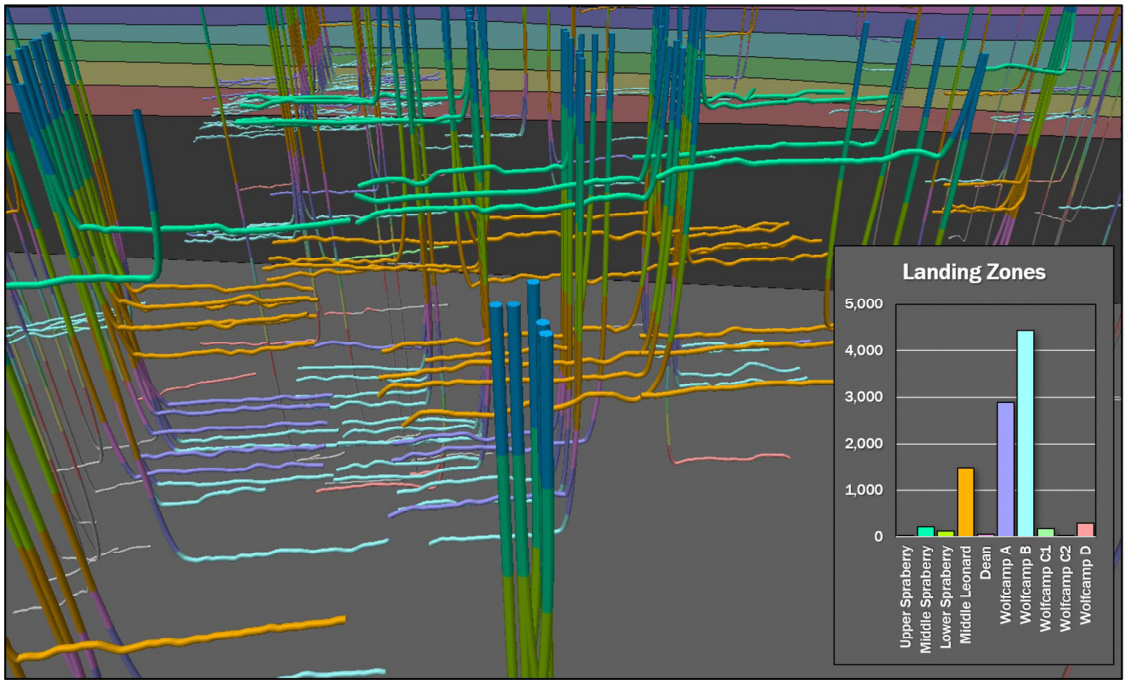

Stratigraphic Zone	Horizontal Wells Landed
Upper Spraberry	26
Middle Spraberry	213
Lower Spraberry	120
Middle Leonard	1,498
Dean	59
Wolfcamp A	2,891
Wolfcamp B	4,445
Wolfcamp C1	176
Wolfcamp C2	29
Wolfcamp D	286
Total Wells landed	9,743

Figure 8. Midland Basin horizontal wells—landing zones. Using the ten 3D model zones of the Spraberry-Wolfcamp interval, the producing horizontal wells were reclassified by landing zone. The colors of the well trajectories change when the well path transitions to a new stratigraphic zone. The corresponding stratigraphic landing zone distribution for the horizontal wells in this study are shown in the histogram.

parameters, and be used to investigate a variety of problems, including for example understanding the drivers of horizontal well performance (Male, 2018)

DISCUSSION AND CONCLUSIONS

Building a 3D geomodel can help integrate a variety of geological data to facilitate refining understanding of basin stratigraphy. The visualization tools available in modern 3D modeling software can enable comprehensive exploration of the data. This can provide new insights and a variety of cross sections, map views and 3D graphics that can be used as tools to test ideas and illustrate concepts. The kind of integrated, multi-faceted, geomodel described in this paper can be used to: estimate the reserves potential by play, by target horizon, and by region; provide an analysis of future production by evaluating the site for future pads, as well as potential infill drilling from existing pads; and to provide a basis for modeling the petroleum systems in the basin.

Over the last few decades, 3D modeling software has had a steep learning curve. These software packages have become more user friendly, though at the same time their range of capabilities and plugin options have increased significantly. As a result, using 3D software solutions, modeling has become labor intensive. However, the power of 3D modeling that gets unleashed by the workflow used in this study, and the strength of the analytical tools available in these modeling packages, more than justify the expensive of time and money involved in developing this capability. Gladczenko et al. (2017) noted that static models can be used to evaluate regional trends as well as provide specific reserves potential in any area. They concluded that integrated 3D models could be used to improve resource development planning with the added ability of keeping the model 'evergreen' by applying history-match type revisions.

Modern 3D geological modeling offers the opportunity to build multiple 3D geological models within a single project, allowing for the creation of multiple scenarios based on different interpretations and parameters. This study has shown the ease in which multiple 3D instances representing varying stratigraphic scales can be constructed for comparison of hydrocarbon reserves-in-place results. The cells in basin-wide models are typically larger than the scale of heterogeneity of the geological data being utilized. Upscaling geology and petrophysical properties such as porosity and permeability has been necessary in the past to enable running models in reasonable time on available desktop computers.

Modern computing, memory, and graphics hardware solutions, combined with state-of-the-art geocellular modeling software, have given us the ability to expand the size and precision of our projects, resulting in the creation of geocellular models with more than one billion cells. The vertical thickness of the cells in these models approaches the resolution of well log curves, limiting the errors related to vertical averaging. High-resolution geocellular models capable of achieving more precise vertical resolutions are better able to capture the stratigraphic complexity of the interbedded siliciclastic and calciclastic layers in the Spraberry and Wolfcamp formations, resulting in more accurate model predictions.

A key contribution of this study is the incorporation of data from large numbers of horizontal wells into building a basin scale geomodel. The first advantage stems from the ability to use the position log trends for the various horizontal well landing zones

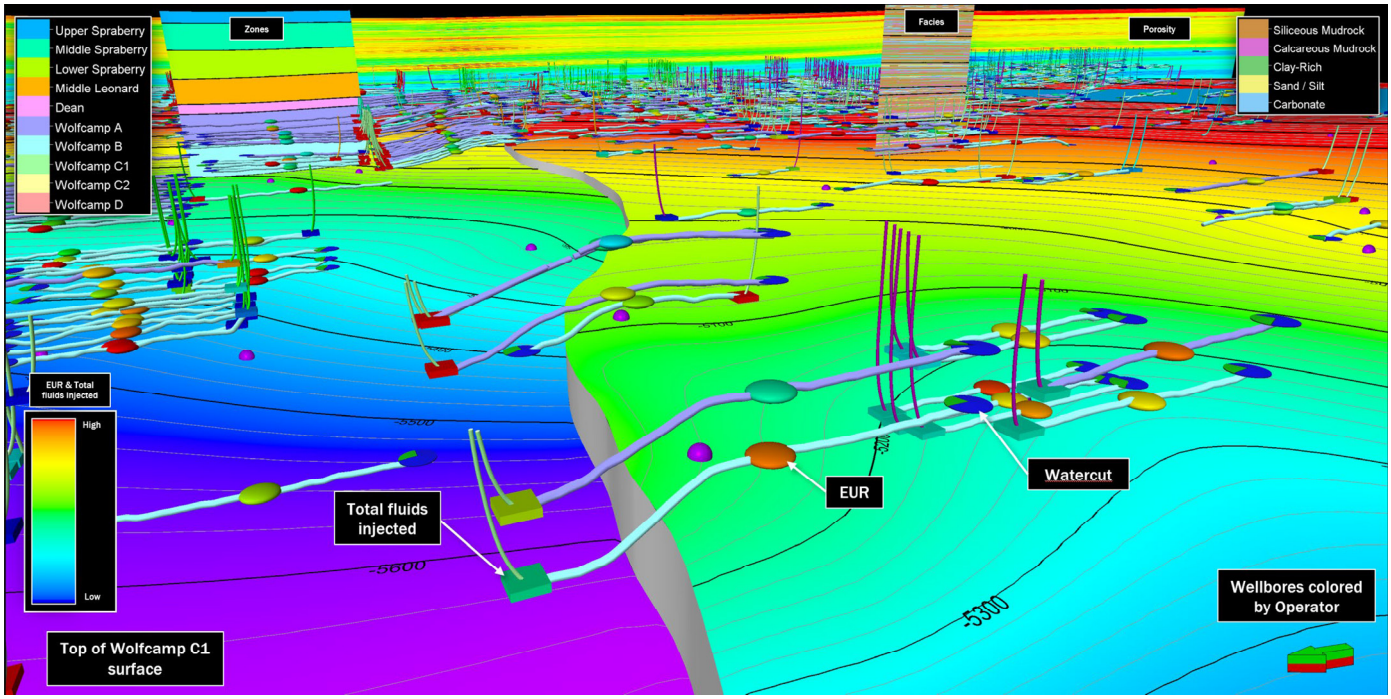

Figure 9. Production and completion data. In this area of the Midland Basin, we illustrate the various production data and completion metrics collected for each of the horizontal wells. The colored surface showing structural contours is the top of the Wolfcamp C1 zone. The well trajectories are colored by different operators. The cube shape at the heel of the well shows colors representing total fluids injected. The 3D ellipsoids at the midpoint of the lateral segment of the well are colored by EUR. The watercut of the well for a particular monthly time-step is shown as a pie diagram at the toe of the wells for which we have production data available. The color of the cylinder along the lateral segment of the well represents the stratigraphic landing zone of the well. In the background we display several cross-sections along several horizontal well trajectories, showing stratigraphic zones and facies. The cross-section shown in the far background shows the distribution of porosity in the zones above the Wolfcamp C1.

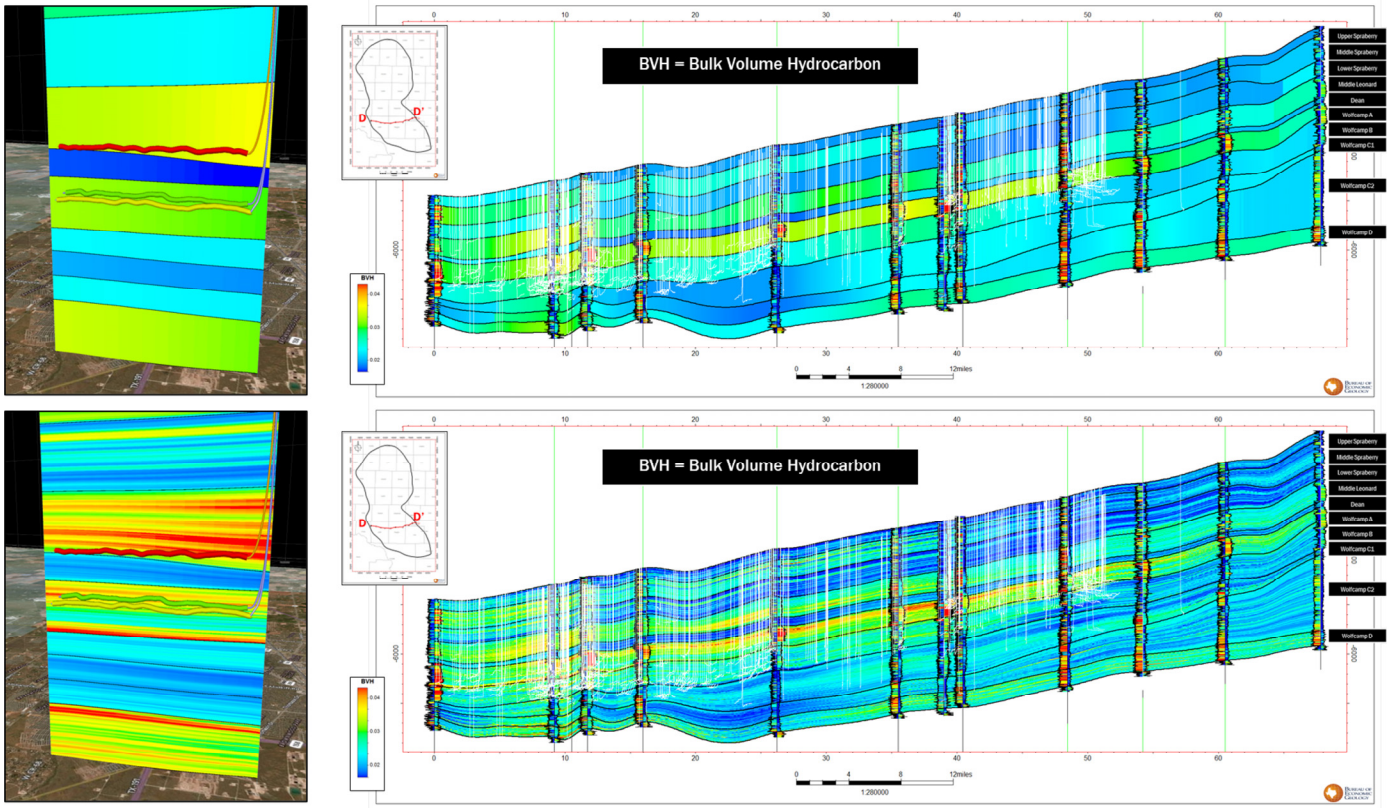

Figure 10. Comparison of vertical and lateral variability of BVH calculations based on two vertical stratigraphic resolution scenarios. The top right cross-section was taken from a single-layer per formation 3D geocellular model, comparable to current 2D mapping-based reserves evaluation studies. The bottom right cross-section was taken from the high-resolution geocellular model. For well logs, the left log curve is gamma ray, increasing to the left, and the right log curve is resistivity, increasing to the right. Horizontal well trajectories are shown as white lines. The two cross-sections on the left show the corresponding vertical resolutions for an area containing multiple stacked horizontal wells. Vertical exaggeration is 20x.

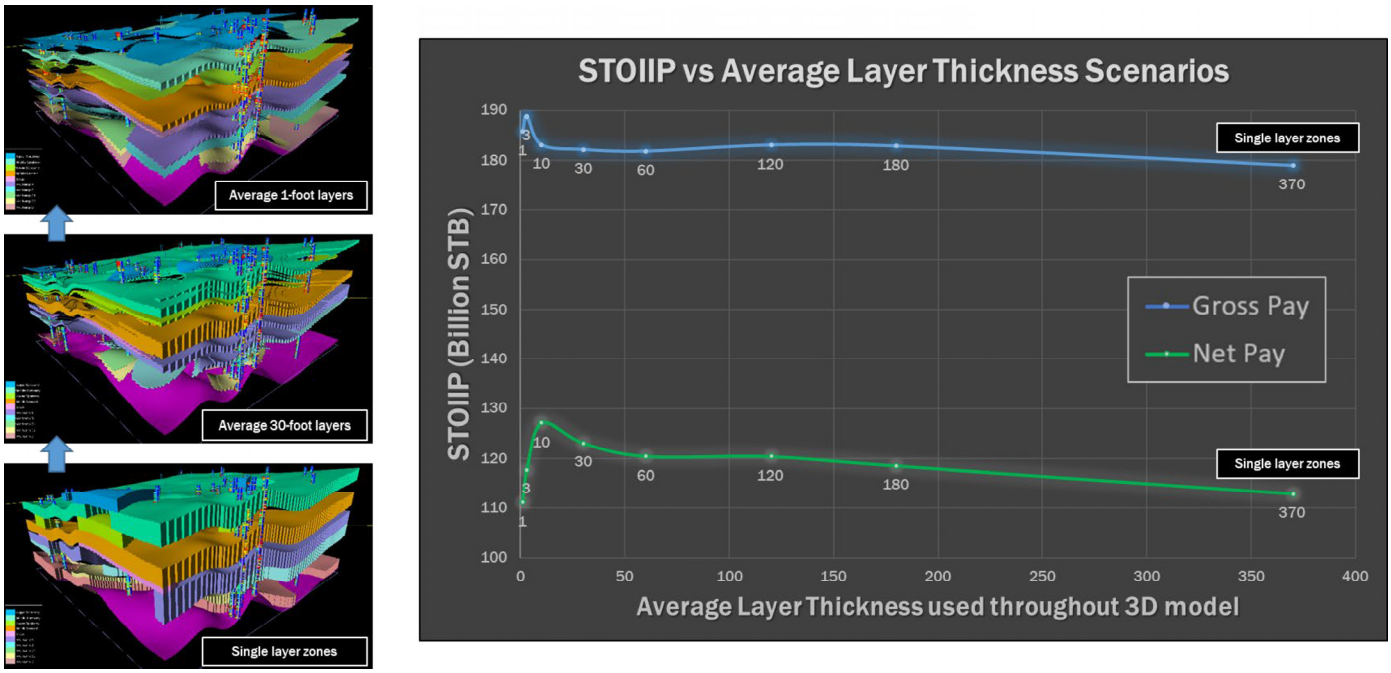

Figure 11. STOIIP by average layer thickness. The graph shows the change of total calculated STOIIP for different vertical layering resolution scenarios. The three images on the left show examples of 3D models showing stratigraphic zones with increasing layer resolution (i.e., decreasing average layer thickness) from the bottom to the top.

to constrain the interwell stratigraphic and structural horizon interpretations. Secondly, the horizontal wells were used to position and distribute pressure and PVT data throughout the model. Finally, the horizontal well trajectories were used to query petrophysical parameters distributed using the well log curves in the vertical wells for subsequent comparison to well productivity parameters like EUR.

More precise STOIIP reserve calculations were obtained in this study by calculating pressures and distributing API gravities at the resolution of the 3D model. This allowed us to implement precise fluid models, resulting in a more accurate distribution of formation volume factors throughout the 3D model.

The STOIIP sensitivity scenarios produced in this study showed that changing the model resolution had a significant influence on the resulting reserves-in-place numbers. This indicates that the higher degree of data-point density we used to construct this 3D geocellular model prevented errors related to over-averaging and is critical to estimating STOIIP accurately, a finding which may significantly impact other basins around the world.

Given the new capabilities of 3D modeling software, reserves assessments can now be based on integrating available data into a digital 3D geomodel. Such models enable the extraction of quantitative data on 3D relationships, testing of hypotheses, and comparing alternative interpretations of the factors controlling well productivity. This paper has presented an argument for the value of providing a multiscale, regional perspective to the practice of 3D reserves assessment geomodeling in the Midland Basin. This 3D model of the Midland Basin will serve as the basis for an extended regional reserves assessment model designed to investigate the relationship between geological facies trends and horizontal well productivity.

ACKNOWLEDGMENTS

Livia Sivila provided analysis of petrophysical data in the Midland Basin. Frank Male provided production data analysis in the form of calculated EUR values for horizontal producers in the Midland Basin. The author thanks Ian Duncan, Frank Male, and Livia Sivila for their valuable insights, suggestions and reviewing previous versions of this paper. The geomodeling projects were partially funded by the BEG STARR, RCRL, and TORA programs. Analysis was performed using the Petrel 3D modeling software obtained through the generous donation to the University of Texas by Schlumberger. This paper is published with the permission of the Director of the BEG.

REFERENCES CITED

Bing Maps, 2022, Permian Basin, aerial with labels, <https://www.bingmapsportal.com>.

Dommisse, R., 2021, Structural and stratigraphic modeling techniques in shale and tight oil basin reservoir studies: Earth ArXiv, <https://doi.org/10.31223/X5V91N>.

Dommisse, R., and C. Kerans, 2021, Characterization and modeling of conventional carbonate systems for enhanced recovery and CCUS: Bureau of Economic Geology Reservoir Characterization Research Laboratory (RCRL), Spring Workshop, 19 May 2021, Austin, Texas, 771 p.

Doveton, J. H., 2014, Principles of mathematical petrophysics: Oxford University Press, UK, 272 p.

Friedrich, M., and G. Monson, 2013, Two practical methods to determine pore pressure regimes in the Spraberry and Wolfcamp formations in the Midland Basin: Unconventional Resources Technology Conference (URTeC), 12–14 August 2013, Denver, Colorado, Paper 1582132, p. 2475–2486, <https://doi.org/10.1190/urtec2013-258>.

Gherabati, S. A., 2018, Material-balance approach for determining drainage volume of multifracture unconventional oil wells: Unconventional Resources Technology Conference (URTeC), 23–25 July 2018, Houston, Texas, Paper 2901597, p. 1784–1798, <https://doi.org/10.15530/urtec-2018-2901597>.

Gladczenko, T., R. Mays, J. Hardt, and M. Houston, 2017, Basin-scale static models for unconventional resource plays, example from Wolfberry in Midland Basin: Unconventional Resources Technology Conference (URTeC), 24–26 July 2017, Austin, Texas, Paper 2697625, p. 3547–3553, <https://doi.org/10.15530/URTEC-2017-2697625>.

Hamlin, H. S., and R. W. Baumgardner, 2012, Wolfberry (Wolfcampian-Leonardian) deep-water depositional systems in the Midland Basin: Stratigraphy, lithofacies, reservoirs, and source rocks: Bureau of Economic Geology Report of Investigations 277, Austin, Texas, 61 p., <https://doi.org/10.23867/RI0277D>.

Heape, A. S., G. Spence, A. Pérez, P. Fonseca, E. Roller, and C. Marin, 2017, Integrated analytical approach identifies Wolfcamp targets outside defined play area: American Oil and Gas Reporter, v. 60, September issue, p. 40–49.

Male, F., C. Aiken, and I. J. Duncan, 2018, Using data analytics to assess the impact of technology change on production forecasting: Society of Petroleum Engineers Paper SPE–191536–MS, Richardson, Texas, 14 p., <https://doi.org/10.2118/191536-MS>.

Male, F., 2019, Using a segregated flow model to forecast production of oil, gas, and water in shale oil plays: Journal of Petroleum Science and Engineering, v. 180, p. 48–61, <https://doi.org/10.1016/j.petrol.2019.05.010>.

Price, B., R. Dommisse, and X. Janson, 2021, Linking depositional environment interpretations and stratal architecture to source rock richness and mechanical property distribution in the Delaware Basin: Unconventional Resources Technology Conference (URTeC), 26–28 July 2021, Houston, Texas, Paper 2021–5108, 12 p., <https://doi.org/10.15530/urtec-2021-5108>.

Ruppel, S. C., ed., 2019, Anatomy of a Paleozoic basin: The Permian Basin, USA: Bureau of Economic Geology Report of Investigations 285, Austin, Texas / American Association of Petroleum Geologists Memoir 118, Tulsa, Oklahoma, v. 1, 412 p., <https://doi.org/10.23867/RI0285-1>.

Ruppel, S. C., ed., 2020, Anatomy of a Paleozoic basin: The Permian Basin, USA: Bureau of Economic Geology Report of Investigations 285, Austin, Texas / American Association of Petroleum Geologists Memoir 118, Tulsa, Oklahoma, v. 2, 538 p., <https://doi.org/10.23867/RI0285-2>.

Sinclair, S. W., L. Crespo, L. Waite, K. Smith, and C. Leslie, 2017, Resource assessment in the northern Midland Basin: Detailed mapping of Late Pennsylvanian, Wolfcampian, and early Leonardian margins and flooding surfaces using well logs and seismic data: Unconventional Resources Technology Conference (URTeC), 24–26 July 2017, Austin, Texas, Paper 2692192, 13 p., <https://doi.org/10.15530/URTEC-2017-2692102>.

Texas Railroad Commission, 2022, Data sets available for download, <https://www.rrc.texas.gov/resource-center/research/data-sets-available-for-download>.